ETH
Eidgenössische Technische Hochschule Zürich
Swiss Federal Institute of Technology Zurich

Solid State Theory
Solution 4

FS 15
PD V. Geshkenbein

Problem 4.1 Brillouin zone of simple crystals

a) **Triangular lattice:**
The Bravais lattice is identical to the crystal lattice. It is generated by vectors

$$\mathbf{a}_1 = a(1,0), \quad \mathbf{a}_2 = \tfrac{a}{2}(1,\sqrt{3}). \tag{1}$$

They are illustrated in the left part of Fig. 1.

The reciprocal lattice is generated by vectors $\mathbf{b}_{1,2}$ such that

$$\mathbf{a}_i \cdot \mathbf{b}_j = 2\pi\delta_{ij}. \tag{2}$$

This definition means that $\mathbf{b}_1 \perp \mathbf{a}_2$ and $\mathbf{b}_2 \perp \mathbf{a}_1$. Direction of vectors $\mathbf{b}_{1,2}$ is found quickly by drawing only. Length of the vectors is fixed by condition (2). Calculation of the dot product reveals that

$$\mathbf{b}_1 = \tfrac{2\pi}{a}\left(1, -\tfrac{1}{\sqrt{3}}\right), \quad \mathbf{b}_2 = \tfrac{4\pi}{a\sqrt{3}}(0,1) \tag{3}$$

so that $|\mathbf{b}_1| = |\mathbf{b}_2| = 4\pi/\sqrt{3}$. Both vectors as well as the generated reciprocal lattice are shown in the right part of Fig. 1. Construction of the first Brillouin zone is also indicated therein.

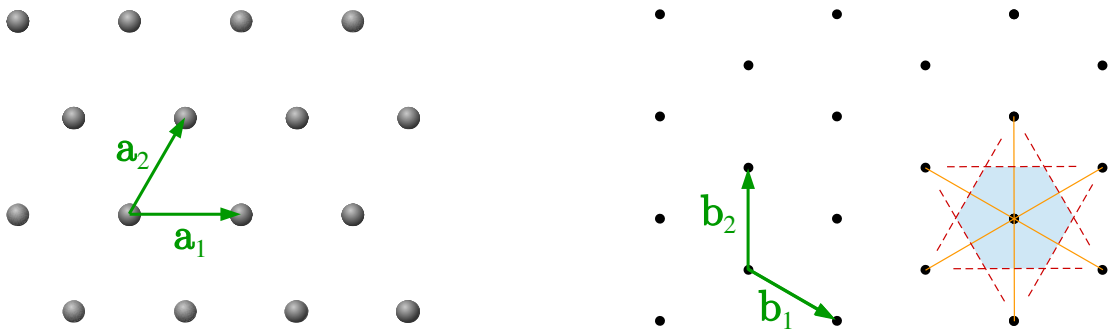

Figure 1: **Left:** Lattice vectors of a triangular lattice. **Right:** The reciprocal lattice to triangular lattice is a triangular lattice. To construct the Brillouin zone around a given point we have to connect it to its nearest neighbours (solid lines). In the next step we draw symmetry axes of these connecting segments (dashed lines). The first Brillouin zone is the interior of the dashed lines, i.e. a hexagon in this case.

b) **Honeycomb lattice:**
A honeycomb lattice is not a Bravais lattice, i.e. there is no pair of vectors $\mathbf{a}_{1,2}$ such that $n_1\mathbf{a}_1 + n_2\mathbf{a}_2, n_{1,2} \in \mathbb{Z}$ would correspond to the lattice sites. In fact, the underlying Bravais lattice is triangular and contains two atoms per lattice site. The lattice vectors are

$$\mathbf{a}_1 = a\left(\sqrt{3}, 0\right), \quad \mathbf{a}_2 = \tfrac{a}{2}\left(\sqrt{3}, 3\right) \tag{4}$$

and are depicted in Fig. 2. Since this is just $\sqrt{3}$-multiple of the lattice vectors in part (a), the corresponding reciprocal vectors are $\sqrt{3}$-times smaller, so that equation (2) would be preserved, i.e.

$$\mathbf{b}_1 = \tfrac{2\pi}{a\sqrt{3}}\left(1, -\tfrac{1}{\sqrt{3}}\right), \quad \mathbf{b}_2 = \tfrac{4\pi}{3a}\,(0,1)\,. \tag{5}$$

The Brillouin zone of a honeycomb lattice has the same shape as for the triangular lattice.

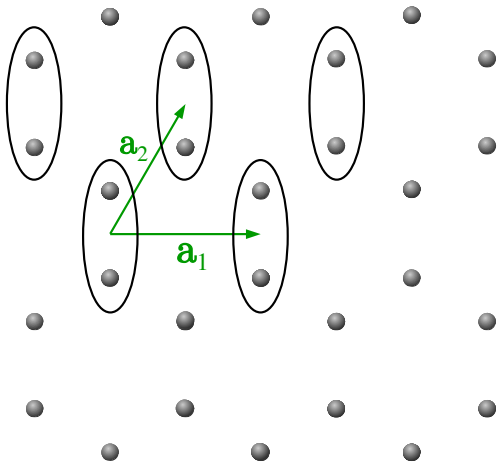

Figure 2: The honeycomb lattice has a triangular Bravais lattice with two sites per unit cell.

b) **Sodium chloride:** The underlying Bravais lattice of this crystal is face-centered cubic with two atoms per unit cell. Vectors that generate the Bravais lattice are

$$\mathbf{a}_1 = a(0,1,1), \quad \mathbf{a}_2 = a(1,0,1), \quad \mathbf{a}_3 = a(1,1,0) \tag{6}$$

and are depicted in the left part of Fig. 3.

Reciprocal lattice is generated by vectors

$$\mathbf{b}_1 = 2\pi\frac{\mathbf{a}_2 \times \mathbf{a}_3}{\mathbf{a}_1 \cdot (\mathbf{a}_2 \times \mathbf{a}_3)} = \tfrac{\pi}{a}\,(-1,1,1) \tag{7}$$

$$\mathbf{b}_2 = 2\pi\frac{\mathbf{a}_3 \times \mathbf{a}_1}{\mathbf{a}_2 \cdot (\mathbf{a}_3 \times \mathbf{a}_1)} = \tfrac{\pi}{a}\,(1,-1,1) \tag{8}$$

$$\mathbf{b}_3 = 2\pi\frac{\mathbf{a}_1 \times \mathbf{a}_2}{\mathbf{a}_3 \cdot (\mathbf{a}_1 \times \mathbf{a}_2)} = \tfrac{\pi}{a}\,(1,1,-1)\,. \tag{9}$$

These vectors generate a body-centered cubic lattice. Its basic building block is depicted in the middle part of Fig. 3. The Brillouin zone has a complicated shape depicted in the right part of the same figure.

Problem 4.2 Two-orbital tight-binding model in 2d

The Bloch-waves constitute a basis of the (quasi-2-dimensional) Hilbert space of the system. Since the Wannier functions are the "Fourier-transforms" of the Bloch-waves, they, too, span the whole Hilbert space. Thus, we can write

$$\mathcal{H} = \sum_{\alpha,\,\alpha',\,\mathbf{j},\,\mathbf{j}'} \langle w_\alpha(\mathbf{r}-\mathbf{r}_\mathbf{j})|\mathcal{H}|w_{\alpha'}(\mathbf{r}-\mathbf{r}_{\mathbf{j}'})\rangle c^\dagger_{\alpha\mathbf{j}} c_{\alpha'\mathbf{j}'}, \tag{10}$$

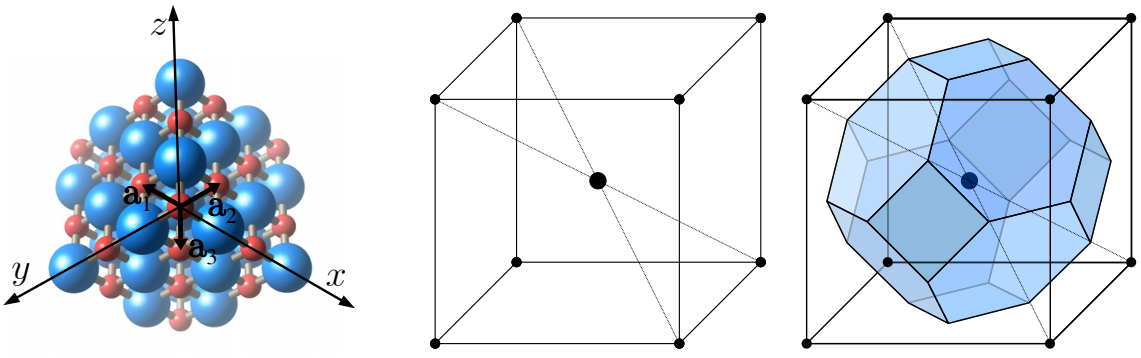

Figure 3: **Left:** Cubic crystal of NaCl crystal viewed along the body diagonal. The dashed lines indicate the underlying face-centered cubic structure. **Middle:** Building block of the reciprocal body-centered cubic lattice. **Right:** The corresponding Brillouin zone.

which can be split in two terms as

$$\mathcal{H} = \sum_{\alpha} \mathcal{H}_{\alpha} + \sum_{\alpha \neq \alpha'} \mathcal{H}_{\alpha,\alpha'}. \tag{11}$$

a) We restrict to the nearest neighbour hopping. The intra-band elements of (10) are

$$\mathcal{H}_{\alpha} = \sum_{\mathbf{j}} \varepsilon_{\alpha} c^{\dagger}_{\alpha\mathbf{j}} c_{\alpha\mathbf{j}} + (t^{x}_{\alpha} c^{\dagger}_{\alpha(\mathbf{j}+\hat{x})} c_{\alpha\mathbf{j}} + t^{y}_{\alpha} c^{\dagger}_{\alpha(\mathbf{j}+\hat{y})} c_{\alpha\mathbf{j}} + \text{h.c.}) \tag{12}$$

with

$$\varepsilon_{\alpha} = \langle w_{\alpha}(\mathbf{r}) | \mathcal{H} | w_{\alpha}(\mathbf{r}) \rangle, \tag{13}$$
$$t^{x}_{\alpha} = \langle w_{\alpha}(\mathbf{r} - a\hat{x}) | \mathcal{H} | w_{\alpha}(\mathbf{r}) \rangle, \tag{14}$$
$$t^{y}_{\alpha} = \langle w_{\alpha}(\mathbf{r} - a\hat{y}) | \mathcal{H} | w_{\alpha}(\mathbf{r}) \rangle. \tag{15}$$

Considering the overlap elements $t^{x,y}_{\alpha}$ for both bands, we recognize that

$$t^{x}_{p_x} = t^{y}_{p_y}, \tag{16}$$
$$t^{x}_{p_y} = t^{y}_{p_x} \tag{17}$$

due to the symmetry properties of the square lattice and of the atomic orbitals. Notice that the inter-band elements

$$\langle w_{\alpha}(\mathbf{r} - a\hat{x}) | \mathcal{H} | w_{\alpha'}(\mathbf{r}) \rangle \quad \text{and} \quad \langle w_{\alpha}(\mathbf{r} - a\hat{y}) | \mathcal{H} | w_{\alpha'}(\mathbf{r}) \rangle \tag{18}$$

are zero to due symmetry reasons. For example, an element

$$\langle w_{p_x}(\mathbf{r} - a\hat{x}) | \mathcal{H} | w_{p_y}(\mathbf{r}) \rangle \tag{19}$$

is zero because $|w_{p_y}(\mathbf{r})\rangle$ is odd under reflection with respect to x-axis, while $\langle w_{p_x}(\mathbf{r} - a\hat{x})|$ is even.

b) We approximate the Wannier functions (which are orthogonal to each other) by atomic (hydrogen) states (which are not orthogonal to each other), and we choose the orientation of the orbitals such that

$$\mathrm{sign}(w_{p_x}(\mathbf{r})) = \begin{cases} \text{positive}, & x > 0, \\ \text{negative}, & x < 0, \end{cases} \tag{20}$$

$$\mathrm{sign}(w_{p_y}(\mathbf{r})) = \begin{cases} \text{positive}, & y > 0, \\ \text{negative}, & y < 0. \end{cases} \tag{21}$$

Using

$$\mathcal{H}_{\mathbf{j}=0}|w_\alpha(\mathbf{r})\rangle = \left(\mathcal{H}_{\mathrm{kin}} + V(\mathbf{r})\right)|w_\alpha(\mathbf{r})\rangle = \left[\varepsilon_\alpha + \sum_{\mathbf{j}\neq 0} V(\mathbf{r}-\mathbf{r}_j)\right]|w_\alpha(\mathbf{r})\rangle, \tag{22}$$

we find for the matrix elements

$$t^x_{p_x} = \langle w_{p_x}(\mathbf{r}-a\hat{x})| \left[\varepsilon_{p_x} + \sum_{\mathbf{j}\neq 0} V(\mathbf{r}-\mathbf{r_j})\right]|w_{p_x}(\mathbf{r})\rangle \tag{23}$$

$$t^y_{p_x} = \langle w_{p_x}(\mathbf{r}-a\hat{y})| \left[\varepsilon_{p_x} + \sum_{\mathbf{j}\neq 0} V(\mathbf{r}-\mathbf{r_j})\right]|w_{p_x}(\mathbf{r})\rangle \tag{24}$$

$$t^x_{p_y} = \langle w_{p_y}(\mathbf{r}-a\hat{x})| \left[\varepsilon_{p_y} + \sum_{\mathbf{j}\neq 0} V(\mathbf{r}-\mathbf{r_j})\right]|w_{p_y}(\mathbf{r})\rangle \tag{25}$$

$$t^y_{p_y} = \langle w_{p_y}(\mathbf{r}-a\hat{y})| \left[\varepsilon_{p_y} + \sum_{\mathbf{j}\neq 0} V(\mathbf{r}-\mathbf{r_j})\right]|w_{p_y}(\mathbf{r})\rangle. \tag{26}$$

Consider first the case of (23) and (26). The main contribution to these matrix elements comes from the region between the two lattice sites where the two orbitals have opposite sign. As $\varepsilon_\alpha < 0$ and $V(\mathbf{r}) < 0$, we obtain that $t^x_{p_x} = t^y_{p_y} > 0$. On the other hand for (24) and (25) the orbitals have the same sign, hence $t^y_{p_x} = t^x_{p_y} < 0$.

Performing the Fourier transformation

$$c_{\alpha\mathbf{j}} = \frac{1}{\sqrt{N}} \sum_{\mathbf{k}} e^{-i\mathbf{k}\cdot\mathbf{r_j}} c_{\alpha\mathbf{k}} \tag{27}$$

of the annihilation operators in the Hamiltonian, we obtain

$$\mathcal{H}_\alpha = \sum_{\mathbf{k}} \varepsilon_{\alpha,\mathbf{k}} c^\dagger_{\alpha\mathbf{k}} c_{\alpha\mathbf{k}} \tag{28}$$

with

$$\varepsilon_{p_x,\mathbf{k}} = \varepsilon + 2t_1\cos(k_x a) - 2t_2\cos(k_y a) \tag{29}$$

$$\varepsilon_{p_y,\mathbf{k}} = \varepsilon - 2t_2\cos(k_x a) + 2t_1\cos(k_y a) \tag{30}$$

where $\varepsilon = \varepsilon_{p_x} = \varepsilon_{p_y}$, $t_1 = t^x_{p_x}$, and $t_2 = -t^y_{p_x} > 0$. The band structure and the Fermi surface for half-filling are visualized in Fig. 4.

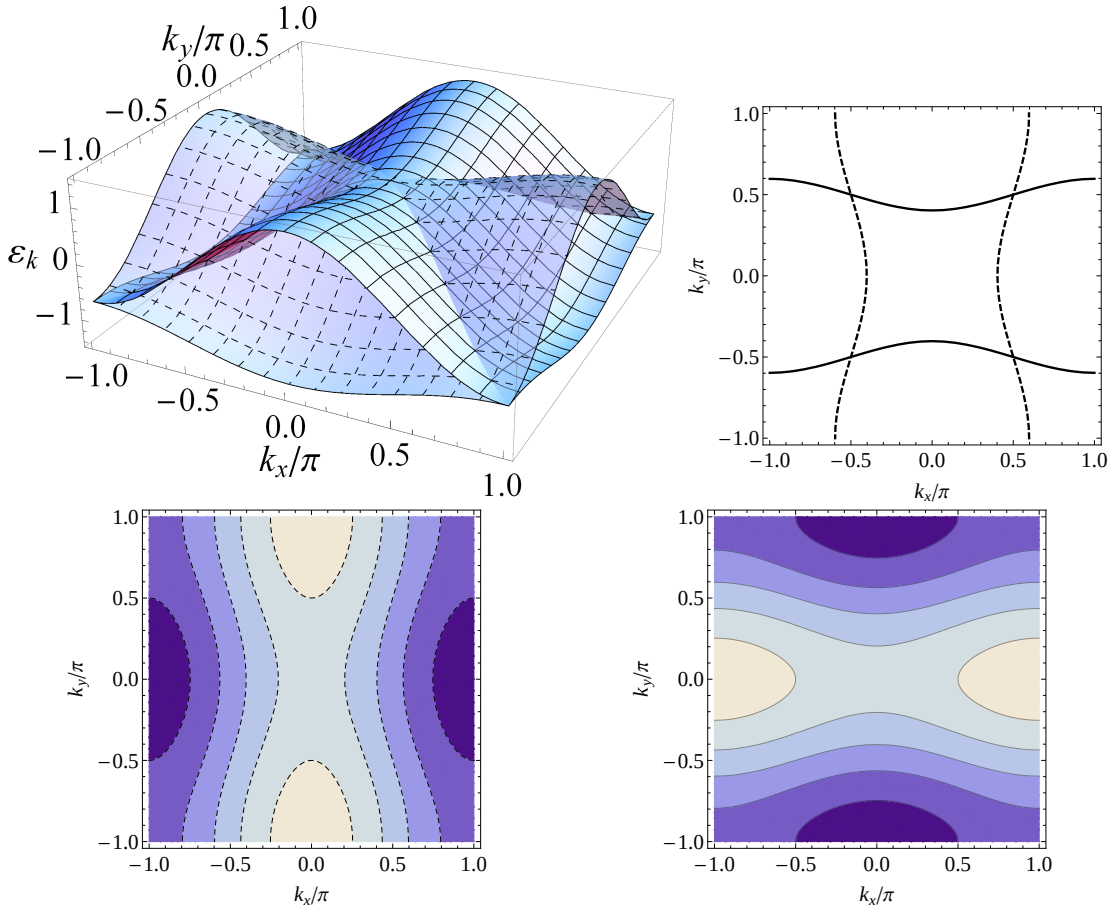

Figure 4: The band structure in the absence of interband coupling is visualized by a 3d plot and contour plot of the two bands. Also shown is the Fermi surface ($t_1 = 0.4, t_2 = 0.1$).

c) We now include the next-nearest neighbour hopping. This modifies part of the Hamiltonian $\mathcal{H}_\alpha$, and it also leads to non-zero $\mathcal{H}_{\alpha,\alpha'}$. We first discuss $\mathcal{H}_\alpha$only, and inter-band coupling will be discussed later.

The next-nearest neighbour contribution to intraband coupling is

$$\tilde{t}_{p_x} = \langle w_{p_x}(\mathbf{r} \pm a\hat{x} \pm a\hat{y})| \left[\varepsilon_{p_x} + \sum_{\mathbf{j}\neq 0} V(\mathbf{r} - \mathbf{r_j})\right] |w_{p_x}(\mathbf{r})\rangle \tag{31}$$

$$\tilde{t}_{p_y} = \langle w_{p_y}(\mathbf{r} \pm a\hat{y} \pm a\hat{y})| \left[\varepsilon_{p_y} + \sum_{\mathbf{j}\neq 0} V(\mathbf{r} - \mathbf{r_j})\right] |w_{p_y}(\mathbf{r})\rangle. \tag{32}$$

Due to lattice symmetries, all four terms in (31) and (32) are equal and $\tilde{t}_{p_x} = \tilde{t}_{p_y} \equiv t_3$. The largest contribution comes from area where the two orbitals have opposite sign, therefore $t_3 > 0$.

Performing a Fourier transformation (27) leads to modified energy bands.

$$\tilde{\varepsilon}_{p_x,\mathbf{k}} = \varepsilon + 2t_1\cos(k_x a) - 2t_2\cos(k_y a) + 4t_3\cos(k_x a)\cos(k_y a) \tag{33}$$

$$\tilde{\varepsilon}_{p_y,\mathbf{k}} = \varepsilon - 2t_2\cos(k_x a) + 2t_1\cos(k_y a) + 4t_3\cos(k_x a)\cos(k_y a). \tag{34}$$

Now we consider the next-nearest neighbour contribution to the interband coupling

$$\mathcal{H}_{\alpha,\alpha'} = \sum_{\mathbf{j}} t^{+}_{\alpha\alpha'} c^{\dagger}_{\alpha(\mathbf{j}+\hat{x}+\hat{y})} c_{\alpha'\mathbf{j}} + t^{-}_{\alpha\alpha'} c^{\dagger}_{\alpha(\mathbf{j}+\hat{x}-\hat{y})} c_{\alpha'\mathbf{j}} + \text{h.c.} \tag{35}$$

with

$$t^{\pm}_{\alpha\alpha'} = \langle w_\alpha(\mathbf{r} - a(\hat{x} \pm \hat{y})|\mathcal{H}|w_{\alpha'}(\mathbf{r})\rangle \tag{36}$$

Due to symmetry properties and the analogue consideration as above, we obtain $t^{+}_{p_x p_y} = t^{+}_{p_y p_x} = -t^{-}_{p_x p_y} = -t^{-}_{p_y p_x} \equiv t_4 > 0$. Performing a Fourier transform of the Hamiltonian, we obtain

$$\mathcal{H}_{\alpha,\alpha'} = \sum_{\mathbf{k}} -4t_4 \sin(k_x a)\sin(k_y a) c^{\dagger}_{\alpha\mathbf{k}} c_{\alpha'\mathbf{k}}. \tag{37}$$

Defining $g_{\mathbf{k}} = -4t_3 \sin(k_x a)\sin(k_y a)$, the complete Hamiltonian can be written as

$$\mathcal{H} = \sum_{\mathbf{k}} \begin{pmatrix} c^{\dagger}_{p_x\mathbf{k}} \\ c^{\dagger}_{p_y\mathbf{k}} \end{pmatrix}^{\mathrm{T}} \begin{pmatrix} \tilde{\varepsilon}_{p_x\mathbf{k}} & g_{\mathbf{k}} \\ g_{\mathbf{k}} & \tilde{\varepsilon}_{p_y\mathbf{k}} \end{pmatrix} \begin{pmatrix} c_{p_x\mathbf{k}} \\ c_{p_y\mathbf{k}} \end{pmatrix} \tag{38}$$

such that to diagonalize the Hamiltonian, we have to find the Eigenvalues $E^{\pm}_{\mathbf{k}}$ of the matrix above determined by the equation

$$(\tilde{\varepsilon}_{p_x\mathbf{k}} - E^{\pm}_{\mathbf{k}})(\tilde{\varepsilon}_{p_y\mathbf{k}} - E^{\pm}_{\mathbf{k}}) - g^2_{\mathbf{k}} = 0. \tag{39}$$

The calculation is straightforward and we obtain

$$E^{\pm}_{\mathbf{k}} = \frac{1}{2}\left[\left(\tilde{\varepsilon}_{p_x\mathbf{k}} + \tilde{\varepsilon}_{p_y\mathbf{k}}\right) \pm \sqrt{\left(\tilde{\varepsilon}_{p_x\mathbf{k}} - \tilde{\varepsilon}_{p_y\mathbf{k}}\right)^2 - g^2_{\mathbf{k}}}\right] \tag{40}$$

The resulting band structure and the Fermi surface for half-filling are plotted in Fig. 5.

d) The p_z orbitals are odd under reflection with respect to xy-plane, while both p_x and p_y orbitals are even. The consequence is that coupling between p_z and $p_{x,y}$ orbitals vanishes in the studied two-dimensional model. The p_z-band thus can be studied independently.

Within the plane the p_z orbitals are effectively s-like. The p_z-band structure can be easily found to be

$$\varepsilon_{p_z\mathbf{k}} = \varepsilon_z - 2t_5\cos(k_x a) - 2t_5\cos(k_y a) - 4t_6\cos(k_x a)\cos(k_y a) \tag{41}$$

where we defined $\varepsilon_{p_z} \equiv \varepsilon_z$ and

$$t_5 = -\langle w_{p_z}(\mathbf{r} \pm a\hat{x})|\left[\varepsilon_{p_x} + \sum_{\mathbf{j}\neq 0} V(\mathbf{r} - \mathbf{r}_{\mathbf{j}})\right]|w_{p_z}(\mathbf{r})\rangle \tag{42}$$

$$= -\langle w_{p_z}(\mathbf{r} \pm a\hat{y})|\left[\varepsilon_{p_x} + \sum_{\mathbf{j}\neq 0} V(\mathbf{r} - \mathbf{r}_{\mathbf{j}})\right]|w_{p_z}(\mathbf{r})\rangle > 0 \tag{43}$$

$$t_6 = -\langle w_{p_z}(\mathbf{r} \pm a\hat{x} \pm a\hat{y})|\left[\varepsilon_{p_x} + \sum_{\mathbf{j}\neq 0} V(\mathbf{r} - \mathbf{r}_{\mathbf{j}})\right]|w_{p_z}(\mathbf{r})\rangle > 0. \tag{44}$$

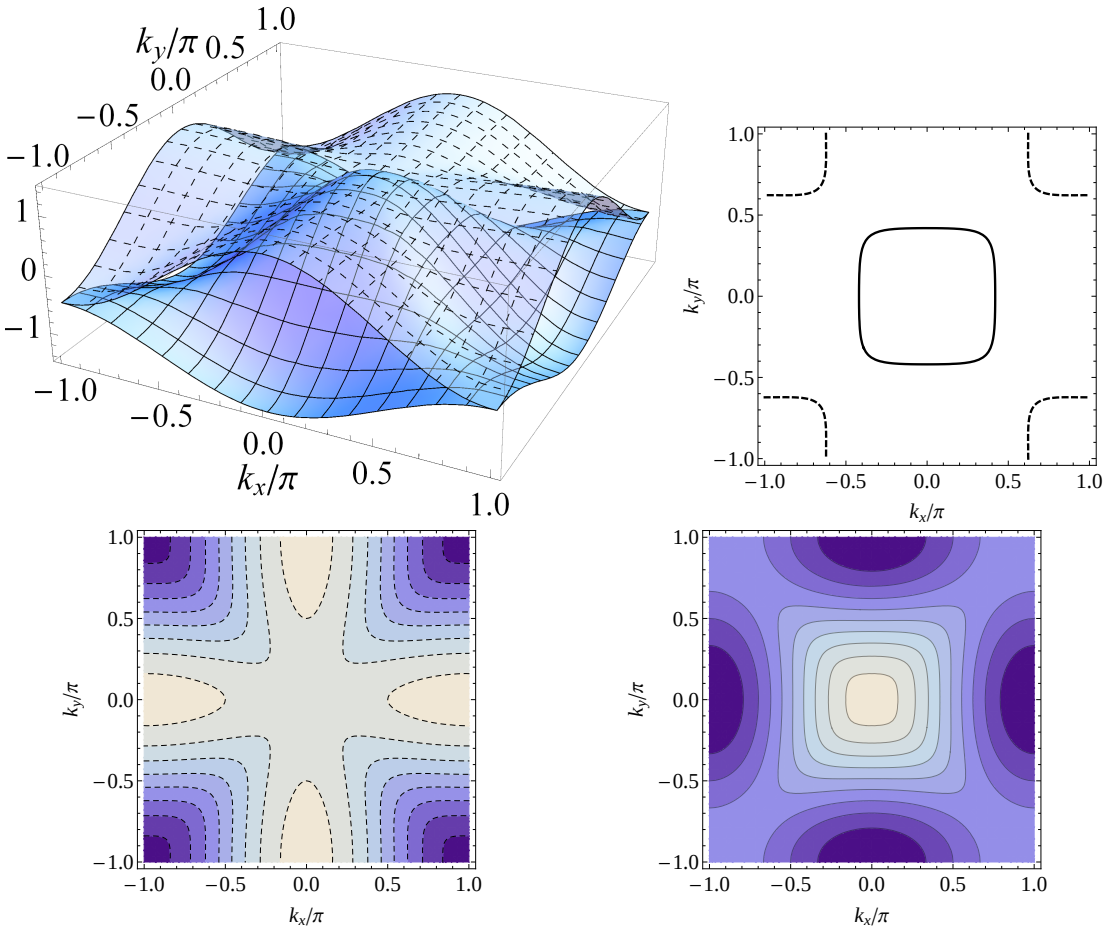

Figure 5: The band structure in the presence of interband coupling is visualized by a 3d plot and contour plot of the two bands. Also shown is the Fermi surface ($t_1 = 0.4$, $t_2 = 0.1$, $t3 = 0.05$, $t_4 = 0.1$).